Science Arts & Métiers (SAM)

is an open access repository that collects the work of Arts et Métiers Institute of Technology researchers and makes it freely available over the web where possible.

To cite this version :

Phenomenological aspects of quasi-perfect pivots in metallic pantographic structures

Mario Spagnuolo [a,*], Patrice Peyre [b], Corinne Dupuy [b]

[a] *International Research Center M&MoCS, Università degli Studi dell'Aquila, L'Aquila, Italy*
[b] *Laboratoire PIMM, Arts et Métiers-ParisTech, CNRS, Cnam, 151 bd de l'Hôpital, Paris 75013, France*

A B S T R A C T

This article discusses the results of the first attempts to print metal pantographic structures with perfect pivots, *i.e.* with rotational hinges connecting the two families of fibers composing the network without any stiffness. On the one hand, it is observed that perfect pivots do not behave as expected theoretically. On the other hand, the force measured during a bias extension test is a few orders of magnitude lower than that measured for pantographic structures with standard pivots (where a certain stiffness is associated to the interconnecting hinges). This leads to considering the pivots as quasi-perfect (non-zero stiffness, but neither the theoretical one which can be computed by means of the geometrical features of the pivot). Numerical simulations complete the analysis by showing how, by modulating the torsional stiffness of the pivots, it is possible to reproduce the force-displacement plot both in the case of standard pivots and with quasi-perfect ones.

1. Introduction

Technological advances in the field of additive manufacturing have made it possible to produce structures and objects with very complex geometry. Because of this peculiar ability, 3D printing has greatly increased the realization and study of metamaterials, i.e. materials that, with a microstructure decided a priori, exhibit exotic mechanical properties. A particular class of metamaterials is represented by the so-called pantographic metamaterials, or pantographic structures. These pantographic structures consist of two families of parallel fibers that are interconnected by some cylinders, called pivots. Recently some samples have been moulded in Polyamide replacing the standard pivots (cylinders with a certain torsional stiffness) with perfect pivots, which correspond to hinges (free rotations). Details of this study are given in [1].

This article introduces for the first time pantographic structures with perfect pivots made of 316L stainless steel. As will be explained below, pivots are not exactly perfect pivots, as residual torsional stiffness is observed experimentally. The dimensions at which the perfect pivot is printed are very close to the precision ensured by the printing and at these levels also the size of the powder used for the printing is a quantity that influences the result. Despite the apparent unsuccess of printing perfect pivot metal

structures, some properties of the specimens, which at first glance are underestimated, can be observed. When comparing the measurements for a standard pivot and a (nominal) perfect pivot specimen, there are considerable differences that can only be ascribed to the different types of pivots. For this reason, they will be referred to as quasi-perfect pivots. An extensive explanation of the process of printing metal pantographic structures is given in [2].

Previous studies had prompted a series of papers (see for example [3–6]) in which the issue of establishing the main exotic characteristics of pantographic metamaterials has been extensively investigated. Several mathematical models have also been advanced, with the purpose of reaching a reasonable compromise between predictive ability and computational practicability. The models can be classified into two categories: (i) discrete, as in [5,7,8], in which a finite collection of rotational and extensional springs is used to describe the complex phenomena of deformation occurring in the microstructure; or (ii) continuous, as in [9–13], which can be ulteriorly differentiated in generalized plate models (of the same kind of those presented e.g. in [14–18]) and in discrete/continuous hybrids, where beams form grids by means of interconnecting pins placed at finite distances (see Boutin et al. [19], Eremeyev et al. [20], Rahali et al. [21], Andreaus et al. [22], Berezovski et al. [23]). The relation between discrete and continuous models can be established by methods of homogenization such as that made in [3,19,24–30].

* Corresponding author.
 E-mail address: mario.spagnuolo.memocs@gmail.com (M. Spagnuolo).

2. Continuum model of pantographic structures

The problems and challenges of designing pantographic structures have been discussed extensively in [31]. The fundamental idea that motivated the development of pantographic metamaterials was to design a metamaterial whose deformation energy is, at first order, a second gradient energy. Similarly to what Casal did in the case of the deformation energy of a beam [32,33], a grid of fibres called pantographic beam [34] was proposed as the fundamental cell of the microstructure to be homogenised to obtain a second gradient macroscopic model with the following properties:

i. it consists of two families of mutually orthogonal fibers, which intersect by means of some cylinders called pivots (see Fig. 1);
ii. the pivots, in theory, have no torsional energy;
iii. an elongation of the structure corresponds (at the first order) to the flexion of the fibers, which is represented by a second gradient energy.

As a result of points (i)–(iii), the homogenised model corresponding to the pantographic beam has, at the first order, a deformation energy which is purely second gradient.

2.1. Deformation energy of a pantographic sheet

In [3] it has been illustrated how to reach a macroscopic model of second gradient continuum by means of a process of homogenization (which actually consists in performing a procedure of identification of the energy of macro-deformation, that is a macroscopic lagrangian density, in terms of constitutive parameters appearing in the postulated expressions of the microdeformation energy) of a postulated micromodel. If we assume a 2D continuum whose reference configuration is given by a rectangular domain $\Omega = [0, L_1] \times [0, L_2] \subset \Re^2$ (for example, in Fig. 1 L_1 and L_2 represent the lengths of the sides of the ideal rectangle which contains the pantographic structure) and assuming the planar motion, the current configuration of Ω is described by the planar macroplacement

$$\chi : \ \Omega \to \Re^2 \tag{1}$$

In [3] it has been shown that the continuum deformation energy of a pantographic structure can be written as

$$\mathcal{U}(\chi(\cdot)) = \int_\Omega \sum_\alpha \frac{K_e}{2}(||\boldsymbol{F}D_\alpha|| - 1)^2 \, d\Omega$$

$$+ \int_\Omega \sum_\alpha \frac{K_b}{2}\left[\nabla \boldsymbol{F}|D_\alpha \otimes D_\alpha \cdot \nabla \boldsymbol{F}|D_\alpha \otimes D_\alpha ||\boldsymbol{F}D_\alpha||^2 \right.$$

$$\left. -\left(\frac{\boldsymbol{F}D_\alpha}{||\boldsymbol{F}D_\alpha||} \cdot \frac{\nabla \boldsymbol{F}|D_\alpha \otimes D_\alpha}{||\boldsymbol{F}D_\alpha||} \right)^2 \right] d\Omega$$

$$+ \int_\Omega \frac{K_p}{2}\left| \arccos\left(\frac{\boldsymbol{F}D_1}{||\boldsymbol{F}D_1||} \cdot \frac{\boldsymbol{F}D_2}{||\boldsymbol{F}D_2||} \right) - \frac{\pi}{2} \right|^\gamma d\Omega \tag{2}$$

In Eq. (2) we used $\boldsymbol{F} = \nabla \chi$ and no sum over repeated α is intended. Since, exploiting [35–39], the pantographic structure can be seen as an assembly of two fiber-reinforced layers connected by the pivots, a last term can be added to Eq. (2) when considering two different placement fields χ^α for the two fiber layers

$$\int_\Omega \frac{K_{int}}{2}||\chi^1 - \chi^2||^2 \, d\Omega \tag{3}$$

It can be interpreted as an interaction term between two co-continuous phases, described by the two placements χ^α, allowing for relative sliding of fibers in correspondence of the inteconnecting pivots. In this work we will neglect the sliding effect, while it has been experimentally observed and theoretically investigated in previous works [22,40].

We can announce that also in the case of the sample with quasi-perfect pivots studied in this article the sliding effect was observed. This is clear in Fig. 2. Nevertheless, the aim of this article is to study the shear features of the pantographic structure and this sliding effect will be treated as a second order effect. For this reason it will be neglected in the study presented here, but it will be the object of next works.

2.2. The shear energy

The third integral in Eq. (2) can be interpreted as a shear deformation energetic contribution at the macro level. At the micro level it may be associated with pivot torsional energy. The form of this energy term depends on the angle between the interconnected fibers by the pivot elevated to a certain power γ: this last parameter can be obtained from experimental data fitting and in general it depends on the type of material in which the structure is fabricated. As will be explained below, the energy of shear can be modeled in other ways too. For example, a model that more accurately captures phenomenology is due to Ogden [41,42]. A version of Ogden shear energy adapted to pantographic structures has been introduced in [43]

$$\mathcal{W}_p(\vartheta, \mathcal{J}) = K_{p1}\left[\left(1 + \left(\frac{\vartheta}{\vartheta_0} \right)^2 \right)^\beta - 1 \right]$$

$$- K_{p2}(\log(\mathcal{J} - \mathcal{J}_0) - (\log(1 - \mathcal{J}_0) - \mathcal{J} + 1) \tag{4}$$

where ϑ is the angle between the fibers in correspondence of the interconnecting pivot and $\mathcal{J}$ the module of its cosinus, while ϑ_0
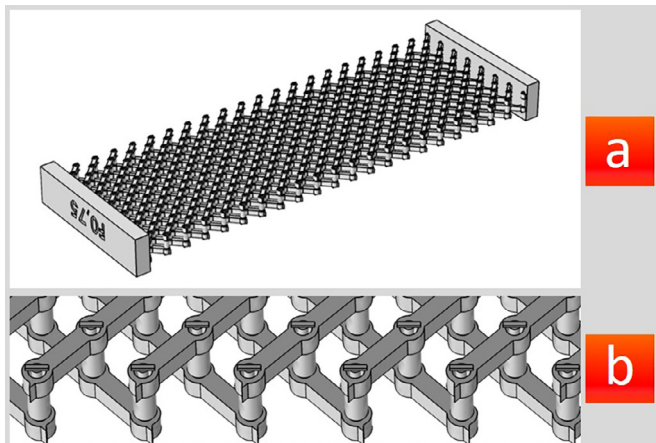

Fig. 1. CAD model of a pantographic structure with perfect-pivots (a). In (b) the perfect pivots are shown.
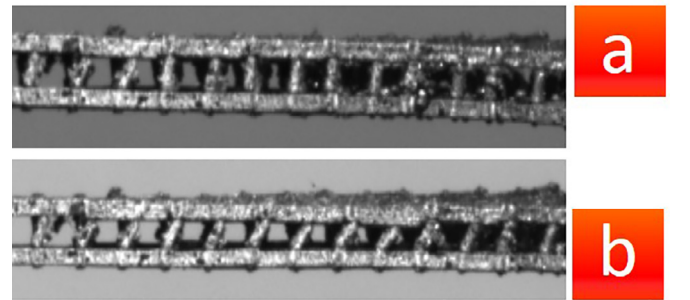

Fig. 2. Experimental observation of the shear of pivots: (a) reference configuration and (b) shear deformation. We are grateful to Dr. X. Pinelli (LMT, ENS Paris-Saclay/CNRS/Université Paris-Saclay) for the photos.
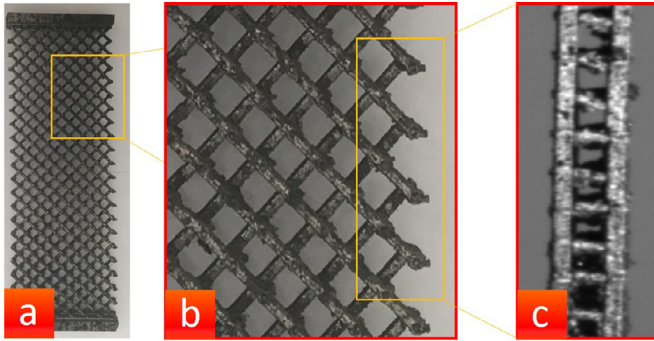
and $\mathcal{J}_0$ are the values of the angle and of its cosinus in some particular points of the deformation history. These last two parameters will be described with more precision in a future work. The two constants K_{pi} $(i = 1, 2)$ substitute the shear stiffness K_p of Eq. (2).

3. Experiments and numerical simulations: quasi-perfect pivots (QPP)

Two specimens, one with standard pivots and one with quasi-perfect pivots, were tested in a bias extension test. The two specimens' shapes are, in the reference configuration, rectangles of sides $L_1 = 30$ mm and $L_2 = 90$ mm. An image of the QPP-sample (Quasi Perfect Pivot sample) can be observed in Fig. 3. Both the specimens are made of 316L stainless steel. Since additive manufacturing does not produce homogeneous but highly porous samples [44,45], the mechanical characteristics of the objects tested must be considered different (lower) than those of the material of which they are made up. The specimens have been created by using the SLM125HL set-up from SLM solutions. This machine is equipped with a 400W YAG laser (YLR-400-WC) at a wavelength of 1070 nm. The scanning speed varies from 400 to 1500 mm/s, while the thickness of the powder layer lies in the range between 30 and 100 µm. The minimum diameter of the laser at the focal point is about 70 µm. The powder employed is 316L stainless steel having spherical particles whose lowest diameter is 37 µm (CILAS 920).The manufacturing of the part is preceded by the proper positioning of the 3D geometry in the printing volume using the MAGICS- Materialize Software.

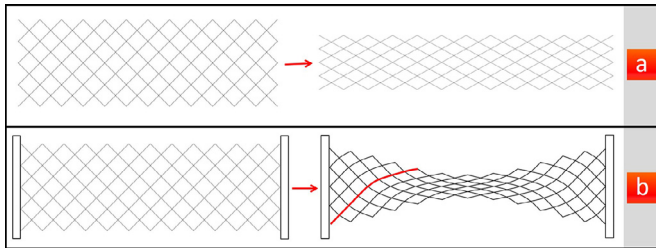**Fig. 3.** QPP specimen (a) and details of the pivots (b,c).

Fig. 4. Schematic description of a bias extension test. (a) A pantographic structure with no clamping deforms without any deformation of the fibers; (b) when the short sides are clamped, the bending of the fibers is observed.

Fig. 5. Comparison between the experimental measurements of reaction force for a pantographic structure with quasi-perfect pivots (blue) and the numerical simulation for a structure with perfect pivots (red, dot-dashed) in which we have posed $K_p = 0$. The numerical simulation is lower than the experimental measure. (For interpretation of the references to colour in this figure legend, the reader is referred to the web version of this article.)

Some further results in the field of metallic additive manufacturing can be found in [46,47].

3.1. Bias extension test in pantographic structures

A bias extension test is the simplest experimental test one can perform on pantographic structures [34] (it is specifically called bias extension and not only extension, because it is performed along a biased direction respect to the fiber direction, see Fig. 4). This particular test is performed by tightening the short sides of the pantographic structure to observe the effects of the second gradient. In fact, as it can be seen in Fig. 4, if the short sides are not blocked, then, in theory, a zero strain energy (a so-called floppy mode) should be measured: up to the point where all the fibers become parallel the extension energy is zero (or negligible). If the short sides are not tightened, the bending energy (second gradient) is also cancelled out. This test was therefore specifically designed to observe the effect of the second gradient in pantographic structures.

3.2. The perfect pivots did not work at a first look

Bias extension tests were performed for the specimen of Fig. 3. The reaction force *versus* prescribed displacement was measured and plotted in Fig. 5. A first remark must be done by observing Fig. 5: by comparing the measured reaction force with the theoretically expected one (obtained via numerical simulation with the prescription that the shear stiffness K_p is zero), it is evident that a substantial part of the deformation energy (the area under the reaction force curve) is missing in the numerical simulated case. In other words, we cannot pose the shear stiffness to zero for the

Table 1
Theoretical expressions for the stiffnesses. E is the Young modulus, G the shear modulus, A the cross-section of the fibers, I the cross-sectional moment of inertia. Finally, p is the interdistance between two pivots on the same fiber, d the diameter and h the height of the pivot.

K_e	K_b	K_p
$EA\backslash p$	$EI\backslash p$	$G\pi d^4\backslash(32hp^2)$

present sample and we cannot say that the pivots are perfect. The theoretical expressions for the stiffnesses used in the numerical simulations are reported in Table 1.

3.3. Comparison with standard pivots

A second comparison must be done, with the experimental curve relative to a bias extension test of a pantographic structure made of the same material (316L stainless steel) but with standard pivots (SP). The comparison of the force-displacement curves for the two specimens is shown in Fig. 6.

An observation can be done immediately. If, on the one hand, it has been remarked that the reaction force measured for the specimen with perfect pivots is significantly higher than that which should be observed if the pivots were really perfect, by comparing it with the curve for the standard pivot specimen, it is clear that the measured force is much lower than in the standard case. In this sense one can conclude that the perfect pivots are not perfect from the microscopic point of view, but they are sufficiently perfect, we say quasi-perfect, from a global macroscopic point of view. The QPP specimen has, infact, a total structural stiffness lower compared to the SP specimen. If the difference between the two
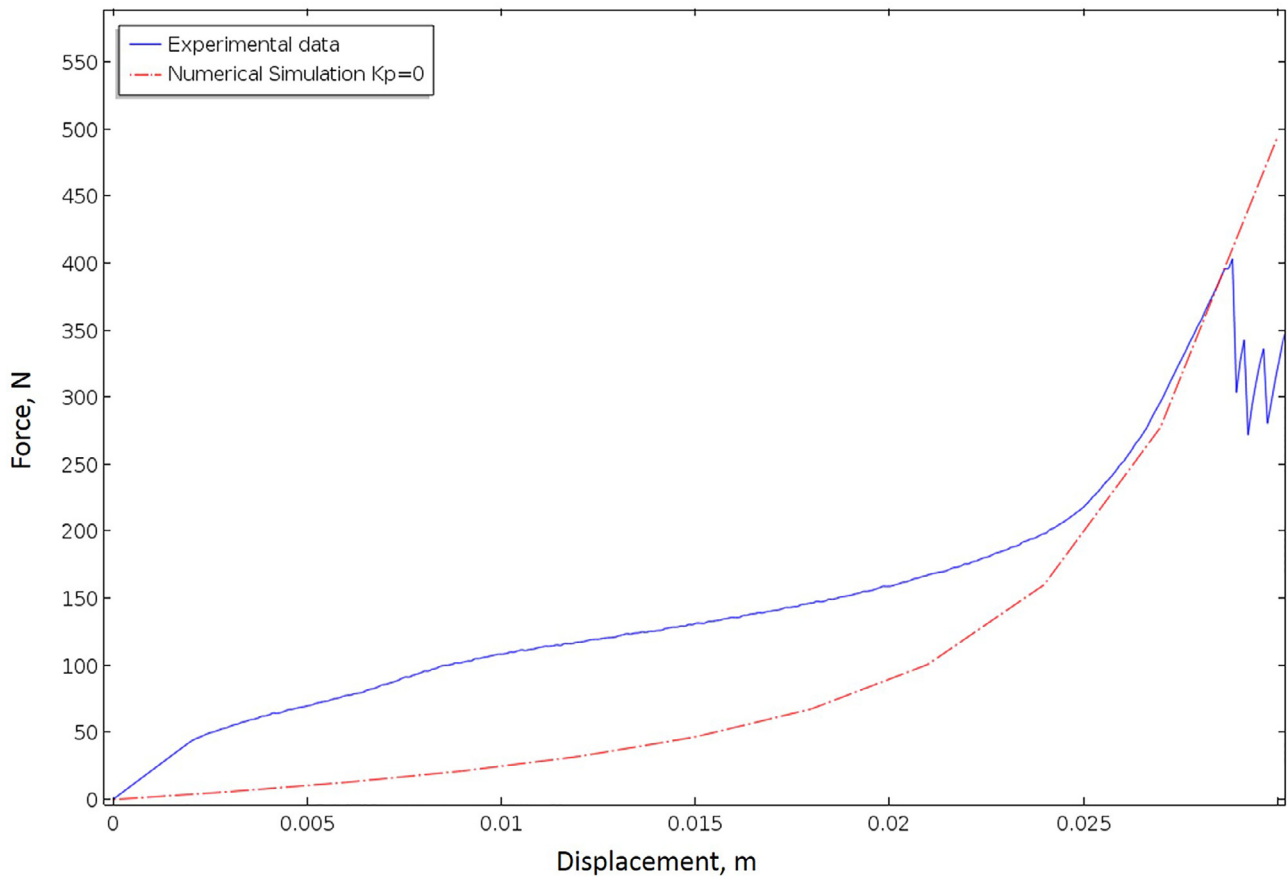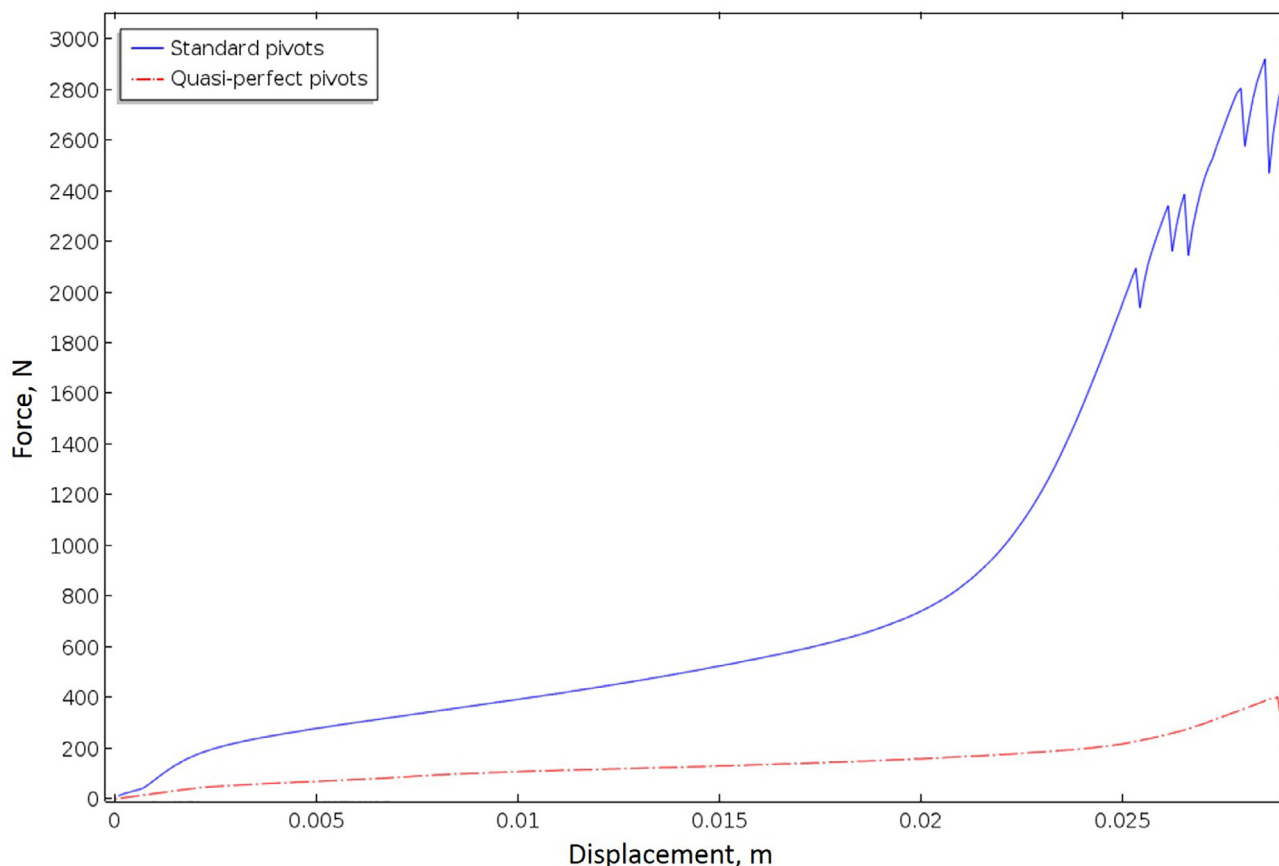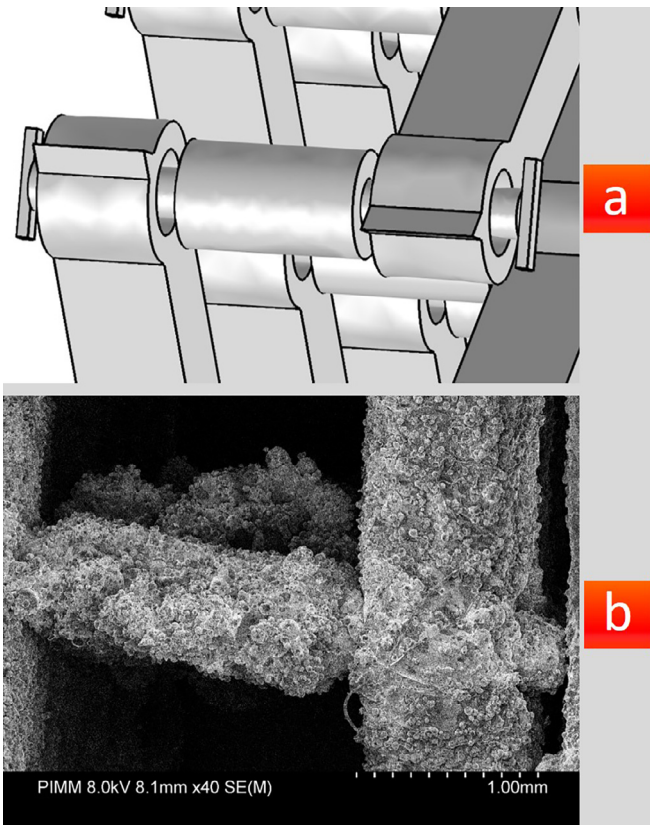

Fig. 6. Comparison between the experimental measurements of reaction force for a pantographic structure with standard pivots (blue) and a structure with quasi-perfect pivots (red, dot-dashed). (For interpretation of the references to colour in this figure legend, the reader is referred to the web version of this article.)

Fig. 7. Comparison betwen the CAD model (a) of a perfect pivot and its practical realisation (b) in 316L stainless steel via additive manufacturing.

has been remarked, the considered pivots are not exactly perfect pivots, as residual torsional stiffness is observed experimentally. This is due to the dimensions at which the perfect pivot is printed (Fig. 7). Despite the apparent unsuccess of printing perfect pivot metal structures, some properties of the specimens, which at first glance are underestimated, have ben observed. When comparing the measurements for a standard pivot and a (nominal) perfect pivot specimen, there are considerable differences that can only be ascribed to the different types of pivots. For this reason, they have been referred to as quasi-perfect pivots.

The study presented can be completed by an analysis of the damage emerging in the quasi-perfect pivots, complementarily to what has been done in [40]. For more general discussions to investigate the damage in higher gradient theories one can refer to [50–53].

A further interesting analysis which can be performed on this kind of structure is the same introduced in [54], where the authors discuss the reversal Poynting effect in metallic pantographic structures. This effect has not been studied when the pivots are perfect. Future analyses will be conducted to fill this gap.

Finally, the polyamide printed pantographic structures with perfect pivots [1] have been used in dynamical studies [55–57]. Once the problems of precision in the printing of perfect pivots will be overcome, it may be worthwhile that similar studies are also carried out on metal specimens.

Declaration of Competing Interest

The authors declare that they have no known competing financial interests or personal relationships that could have appeared to influence the work reported in this paper.

Acknowledgement

References

[1] E. Turco, A. Misra, M. Pawlikowski, F. dell'Isola, F. Hild, Enhanced Piola–Hencky discrete models for pantographic sheets with pivots without deformation energy: numerics and experiments, Int. J. Solids Struct. (2018).

[2] M. De Angelo, M. Spagnuolo, F. D'Annibale, A. Pfaff, K. Hoschke, A. Misra, C. Dupuy, P. Peyre, J. Dirrenberger, M. Pawlikowski, The macroscopic behavior of pantographic sheets depends mainly on their microstructure: experimental evidence and qualitative analysis of damage in metallic specimens, Contin. Mech. Thermodyn. (2019) 1–23.

[3] F. dell'Isola, I. Giorgio, M. Pawlikowski, N. Rizzi, Large deformations of planar extensible beams and pantographic lattices: heuristic homogenization, experimental and numerical examples of equilibrium, Proc. R. Soc. A 472 (2185) (2016) 20150790.

[4] D. Steigmann, F. dell'Isola, Mechanical response of fabric sheets to three-dimensional bending, twisting, and stretching, Acta Mechanica Sinica 31 (3) (2015) 373–382.

[5] E. Turco, F. dell'Isola, A. Cazzani, N. Rizzi, Hencky-type discrete model for pantographic structures: numerical comparison with second gradient continuum models, Z. Angew. MathPhys. 67 (2016).

[6] F. dell'Isola, T. Lekszycki, M. Pawlikowski, R. Grygoruk, L. Greco, Designing a light fabric metamaterial being highly macroscopically tough under directional extension: first experimental evidence, Z. Angew. Math. Phys. 66 (2015) 3473–3498.

[7] E. Turco, I. Giorgio, A. Misra, F. dell'Isola, King post truss as a motif for internal structure of (meta) material with controlled elastic properties, Royal Soc. Open Sci. 4 (10) (2017) 171153.

[8] I. Giorgio, N. Rizzi, E. Turco, Continuum modelling of pantographic sheets for out-of-plane bifurcation and vibrational analysis, Proc. R. Soc. A 473 (2207) (2017) 20170636.

[9] I. Giorgio, Numerical identification procedure between a micro-cauchy model and a macro-second gradient model for planar pantographic structures, Z. Angew. Math. Phys. 67 (95) (2016).

[10] L. Placidi, E. Barchiesi, E. Turco, N.L. Rizzi, A review on 2D models for the description of pantographic fabrics, Z. Angew. Math. Phys. 67 (5) (2016) 121.

mechanical behaviors is ascribed solely to the pivots, then it makes sense to examine the ratio between the shear stiffnesses of the two specimens. Both the values are identified by using the theoretical expressions in Table 1. We obtain

$$\frac{K_p(QPP)}{K_p(SP)} = 0.1 \tag{5}$$

We can therefore conclude that the manufacturing process of perfect pivots has been partially successful, having produced pivots with torsional stiffness of an order of magnitude lower than the case of standard pivots. The reason for the incomplete success of the perfect pivots can be easily understood by observing Fig. 7 in which the CAD design of a perfect pivot and its realization by additive manufacturing are compared. The photo shows precisely the porosity that prevents the mechanism of the perfect pivot from working properly. In the phase of fabrication, the specimens were positioned orthogonally to the building platform even though a tilt angle of 45° would have been preferable for the realization of the pivots. Despite the significant technological achievements represented by such manufacturing technologies, the objects obtained are very sensitive to the location and the number of supports whose inadequate positioning could result in widespread microstructural flaws. Furthermore, the rough surfaces in Fig. 7b show porosity which can potentially be suppressed by heat treatments such as Hot Isostatic Pressing (HIP), resulting in almost-fully dense metallic alloys [47] (such post processing was not performed on the samples). Useful information about the heat treatment effects on transformation strain in steels can be found in [48,49].

4. Conclusion

In this article pantographic structures with perfect pivots made of 316L stainless steel have been studied for the first time. As it

[11] E. Barchiesi, L. Placidi, A review on models for the 3D statics and 2D dynamics of pantographic fabrics, in: Wave Dynamics and Composite Mechanics for Microstructured Materials and Metamaterials, Springer, 2017, pp. 239–258.

[12] E. Barchiesi, G. Ganzosch, C. Liebold, L. Placidi, R. Grygoruk, W.H. Müller, Out-of-plane buckling of pantographic fabrics in displacement-controlled shear tests: experimental results and model validation, Contin. Mech. Thermodyn. (2018) 1–13.

[13] E. Barchiesi, F. dell'Isola, M. Laudato, L. Placidi, P. Seppecher, A 1d continuum model for beams with pantographic microstructure: asymptotic micro-macro identification and numerical results, in: Advances in Mechanics of Microstructured Media and Structures, Springer, 2018, pp. 43–74.

[14] H. Altenbach, V. Eremeyev, On the linear theory of micropolar plates, ZAMM-J. Appl. Math.Mech. 89 (4) (2009) 242–256.

[15] W. Pietraszkiewicz, V. Eremeyev, On natural strain measures of the non-linear micropolar continuum, Int. J. Solids Struct. 46 (3) (2009) 774–787.

[16] V.A. Eremeyev, W. Pietraszkiewicz, Material symmetry group and constitutive equations of micropolar anisotropic elastic solids, Math. Mech. Solids 21 (2) (2016) 210–221.

[17] V.A. Eremeyev, W. Pietraszkiewicz, Local symmetry group in the general theory of elastic shells, J. Elast. 85 (2) (2006) 125–152.

[18] V.A. Eremeyev, On the material symmetry group for micromorphic media with applications to granular materials, Mech. Res. Commun. 94 (2018) 8–12.

[19] C. Boutin, I. Giorgio, L. Placidi, et al., Linear pantographic sheets: asymptotic micro-macro models identification, Math. Mech. Complex Syst. 5 (2) (2017) 127–162.

[20] V.A. Eremeyev, F. dell'Isola, C. Boutin, D. Steigmann, Linear pantographic sheets: existence and uniqueness of weak solutions, J. Elast. (2017) 1–22.

[21] Y. Rahali, I. Giorgio, J. Ganghoffer, F. dell'Isola, Homogenization à la piola produces second gradient continuum models for linear pantographic lattices, Int. J. Eng. Sci. 97 (2015) 148–172.

[22] U. Andreaus, M. Spagnuolo, T. Lekszycki, S.R. Eugster, A ritz approach for the static analysis of planar pantographic structures modeled with nonlinear euler–bernoulli beams, Contin. Mech. Thermodyn (2018) 1–21.

[23] A. Berezovski, I. Giorgio, A.D. Corte, Interfaces in micromorphic materials: wave transmission and reflection with numerical simulations, Math. Mech. Solids 21 (1) (2016) 37–51.

[24] B. Abali, W. Müller, F. dell'Isola, Theory and computation of higher gradient elasticity theories based on action principles, Arch. Appl. Mech. (2017) 1–16.

[25] J.-J. Alibert, P. Seppecher, F. dell'Isola, Truss modular beams with deformation energy depending on higher displacement gradients, Math. Mech. Solids 8 (1) (2003) 51–73.

[26] M. Camar-Eddine, P. Seppecher, Closure of the set of diffusion functionals with respect to the mosco-convergence, Math. Models Methods Appl. Sci. 12 (08) (2002) 1153–1176.

[27] M. Camar-Eddine, P. Seppecher, Determination of the closure of the set of elasticity functionals, Arch. Appl. Mech. Anal. 170 (3) (2003) 211–245.

[28] M. Camar-Eddine, P. Seppecher, Non-local interactions resulting from the homogenization of a linear diffusive medium, Comptes Rendus de l'Académie des Sciences-Series I-Mathematics 332 (5) (2001) 485–490.

[29] A. Carcaterra, F. dell'Isola, R. Esposito, M. Pulvirenti, Macroscopic description of microscopically strongly inhomogeneous systems: a mathematical basis for the synthesis of higher gradients metamaterials, Arch. Appl. Mech. Anal. 218 (3) (2015) 1239–1262.

[30] N. Challamel, A. Kocsis, C. Wang, Higher-order gradient elasticity models applied to geometrically nonlinear discrete systems, Theor. Appl. Mech. 42 (4) (2015) 223–248.

[31] F. dell'Isola, P. Seppecher, J.J. Alibert, T. Lekszycki, R. Grygoruk, M. Pawlikowski, D. Steigmann, I. Giorgio, U. Andreaus, E. Turco, et al., Pantographic metamaterials: an example of mathematically driven design and of its technological challenges, Contin. Mech. Thermodyn. (2018) 1–34.

[32] P. Casal, La capillarité interne, Cahier Groupe Français rhéol. CNRS VI 3 (1961) 31–37.

[33] P. Casal, Theory of second gradient and capillarity, C. R. Hebd. Séances Acad. Sci. A 274 (22) (1972) 1571.

[34] P. Seppecher, J.-J. Alibert, F. dell'Isola, Linear elastic trusses leading to continua with exotic mechanical interactions, in: Journal of Physics: Conference Series, 319, IOP Publishing, 2011, p. 012018.

[35] P. Franciosi, Laminate system schemes for effective property estimates of architectured composites with co-(dis) continuous phases, Mech. Res. Commun. 45 (2012) 70–76.

[36] P. Franciosi, A. El Omri, Effective properties of fiber and platelet systems and related phase arrangements in n-phase heterogenous media, Mech. Res. Commun. 38 (1) (2011) 38–44.

[37] P. Franciosi, H. Lebail, Anisotropy features of phase and particle spatial pair distributions in various matrix/inclusions structures, Acta Mater. 52 (10) (2004) 3161–3172.

[38] P. Franciosi, A regularized multi-laminate-like plasticity scheme for poly-crystals, applied to the fcc structure, Procedia IUTAM 3 (2012) 141–156.

[39] P. Franciosi, Multiple continuity of phases in composite materials: overall property estimates from a laminate system scheme, Int. J. Solids Struct. (2019).

[40] M. Spagnuolo, K. Barcz, A. Pfaff, F. dell'Isola, P. Franciosi, Qualitative pivot damage analysis in aluminum printed pantographic sheets: numerics and experiments, Mech. Res. Commun. 83 (2017) 47–52.

[41] R. Ogden, P. Chadwick, E. Haddon, Combined axial and torsional shear of a tube of incompressible isotropic elastic material, Quart. J. Mech. Appl. Math. 26 (1) (1973) 23–41.

[42] R.W. Ogden, Non-linear Elastic Deformations, Courier Corporation, 1997.

[43] I. Giorgio, P. Harrison, F. dell'Isola, J. Alsayednoor, E. Turco, Wrinkling in engineering fabrics: a comparison between two different comprehensive modelling approaches, Proc. Royal Soc. A 474 (2216) (2018) 20180063.

[44] J. Čapek, M. Machova, M. Fousova, J. Kubásek, D. Vojtěch, J. Fojt, E. Jablonska, J. Lipov, T. Ruml, Highly porous, low elastic modulus 316l stainless steel scaffold prepared by selective laser melting, Mater. Sci. Eng. 69 (2016) 631–639.

[45] A. Haboudou, P. Peyre, A. Vannes, Study of keyhole and melt pool oscillations in dual beam welding of aluminum alloys: effect on porosity formation, in: First International Symposium on High-Power Laser Macroprocessing, 4831, International Society for Optics and Photonics, 2003, pp. 295–301.

[46] V. Gunenthiram, P. Peyre, M. Schneider, M. Dal, F. Coste, R. Fabbro, Analysis of laser–melt pool–powder bed interaction during the selective laser melting of a stainless steel, J. Laser Appl. 29 (2) (2017) 022303.

[47] O. Andreau, I. Koutiri, P. Peyre, J.-D. Penot, N. Saintier, E. Pessard, T. De Terris, C. Dupuy, T. Baudin, Texture control of 316l parts by modulation of the melt pool morphology in selective laser melting, J. Mater. Process. Technol. 264 (2019) 21–31.

[48] T. Otsuka, D. Satani, K. Yamamoto, K. Okamura, R. Brenner, B. Bacroix, Microstructure and heat treatment effect on transformation strain in steels: part 1 experiment, Mater. Sci. Technol. 35 (2) (2019) 181–186, doi:10.1080/02670836.2018.1548110.

[49] T. Otsuka, D. Satani, K. Yamamoto, K. Okamura, R. Brenner, B. Bacroix, Microstructure and heat treatment effect on transformation strain in steels: part 2 modelling, Mater. Sci. Technol. 35 (2) (2019) 187–194, doi:10.1080/02670836.2018.1548111.

[50] L. Placidi, E. Barchiesi, Energy approach to brittle fracture in strain-gradient modelling, Proc. R. Soc. A 474 (2210) (2018) 20170878.

[51] L. Placidi, A. Misra, E. Barchiesi, Two-dimensional strain gradient damage modeling: a variational approach, Z. Angew. Math. Phys. 69 (3) (2018) 56.

[52] L. Placidi, E. Barchiesi, A. Misra, A strain gradient variational approach to damage: a comparison with damage gradient models and numerical results, Math. Mech. Complex Syst. 6 (2) (2018) 77–100.

[53] L. Placidi, A. Misra, E. Barchiesi, Simulation results for damage with evolving microstructure and growing strain gradient moduli, Contin. Mech. Thermodyn. (2018) 1–21.

[54] A. Misra, T. Lekszycki, I. Giorgio, G. Ganzosch, W.H. Müller, F. dell'Isola, Pantographic metamaterials show atypical poynting effect reversal, Mech. Res. Commun. 89 (2018) 6–10.

[55] M. Laudato, L. Manzari, E. Barchiesi, F. Di Cosmo, P. Göransson, First experimental observation of the dynamical behavior of a pantographic metamaterial, Mech. Res. Commun. 94 (2018) 125–127.

[56] E. Barchiesi, M. Laudato, F. Di Cosmo, Wave dispersion in non-linear pantographic beams, Mech. Res. Commun. 94 (2018) 128–132.

[57] M. Laudato, F. Di Cosmo, R. Drobnicki, P. Göransson, Dynamical vector fields on pantographic sheet: Experimental observations, in: New Achievements in Continuum Mechanics and Thermodynamics, Springer, 2019, pp. 257–269.